Fibers and Polymers 2019, Vol.20, No.6, 1301-1310
DOI 10.1007/s12221-019-1008-0

ISSN 1229-9197 (print version)
ISSN 1875-0052 (electronic version)

The Effect of Single and Double-wefted Styles on the In-plane Impact Behavior of Fabric Carbon-aramid/Epoxy Intralayer Hybrid Composite Laminates

Jiaojiao Xi, Jingyun Yu, and Zhiqiang Yu*

Department of Materials Science, Fudan University, Shanghai 200433, China
(Received October 29, 2018; Revised February 3, 2019; Accepted February 10, 2019)

Abstract: The characterization of in-plane impact properties of epoxy laminates reinforced with intralayer hybrid carbon/aramid fabrics was investigated. The effects of different fabrics, which had architectures of 2D and 3D form, on the impact performance was analyzed by drop-weight impact test. It revealed that different braiding styles had a significant influence on the impact properties. The anti-impact properties were enhanced due to aramid fibers into fabrics, in particular, the fabrics with 3D styles that aramid fibers as the Z-yarns. Laminates reinforced by 3D fabrics containing 25 % aramid fiber presented optimal anti-impact performance, and impact peak force and absorbed energy reached 4217 N and 26.71 J, increased by 135.5 % and 137.2 % relative to pure carbon fabric system, respectively. The results of damage morphologies showed that main damage modes, of fiber kinking, necking and fracture, improved the cushioning effect of laminates, which contributed to the enhancement of impact resistance capacity of composite laminates.

Keywords: 2D&3D intralayer hybrid fabrics, Carbon/aramid-epoxy laminates, Double-wefted method, In-plane impact performance, Damage mechanism

Introduction

Carbon fiber reinforced composite laminates have been used in various applications including aerospace, defense and automobiles that are subjected to impact loading during in-service conditions due to their superior mechanical properties [1-4]. Numerous investigation about mechanical performance of composite laminates under tensile, compression and bending load have been carried out [5-10]. However, the characterization of carbon fiber reinforced composites under in-plane impact is still in infancy. Some accidents caused by sudden impact, from hailstones, lightning strike, bird impact, ice shedding and runway debris, frequently occur, which can cause impact damage such as delamination, matrix cracking and fiber fracture, bringing about a decrease of load carrying capacity of the carbon composite laminates [11-15]. The investigation of improving impact resistance of composite laminates will enable to develop better models for various impact loadings. In past few years, many researchers have focused on improving impact damage tolerance of composite laminate by incorporating other fiber such as aramid fibers, glass fibers and nanofibers [16-20]. Jun Hee Song realized the improvement of impact resistance by designing the interlayer hybrid two-dimensional (2D) composites with lamination pairing of carbon/aramid fiber, due to a toughening mechanism of aramid fiber. However, the delamination failure between plies of composite laminates even at very low impact loads restricts its further development [21]. The problem about easier delamination failure of composite laminates made up by stacking design also is proved by the literatures [22-25]. For solving above problem, other strategies are proposed to improve the damage tolerance of composite laminates under impact loads, for example, intralayer hybrid laminates reinforced by 2D braiding architecture fabrics [26-28]. The in-plane impact properties of 2D laminates reinforced with aramid/basalt fabrics are investigated, and results show that the impact damage resistance of composite laminate is significantly enhanced relative to the interlayer hybrid composite [29]. However, the application of 2D laminates with braiding architecture fabrics in high energy impact field is further restricted due to itself lower impact damage resistance and interlaminar shear strength performance [30,31]. Therefore, three-dimensional (3D) textile composites, with higher through-thickness properties and energy absorption capacity, have a promising prospect in engineering fields, because of the superior performance along thickness direction [32-34]. Seltzer *et al*. showed that the specific energy absorbed by 3D braiding composites is twice higher than that of 2D laminates for carbon-glass braiding composites [35]. Li *et al*. [36] investigated the impact damage characterizations of 3D braiding composite and found that the energy absorption greatly increases due to the effect of energy dissipation path in thickness direction. However, the complexity of manufacturing technology and higher cost restrict the 3D braiding composite more extensive applications. With aiming at combining the benefits of superior performance along thickness direction from 3D fabrics and lower processing cost of 2D braid composite laminates, the 3D braiding composite laminates with through-thickness properties by easier process has been research hotspot. Thus, to obtain 3D intralayer hybrid laminates with superior impact damage resistance performance, double-wefted method of a novel braiding technology is employed in some investigations [37,38]. For example, the compressive response of composite laminates reinforced by Z-pinned braiding glass fiber textile

*Corresponding author: yuzhiqiang@fudan.edu.cn

is investigated [39].

As reported in previous literatures, the investigations are mainly focused on the mechanical performance of composite laminates reinforced by 2D&3D braiding fabric under tensile, compression and bending load. However, it has not been fully reported yet about mechanical performance and damage mechanism of composite laminate under impact loads, in particular, the composite laminates reinforced by 3D braiding fabrics with double-wefted method, which exists aramid fibers as Z-yarns in the thickness direction. In this paper, the intralayer hybrid fabrics with carbon and aramid fibers, which have architectures of 2D and 3D form by easier method in terms of single and double-wefted method, respectively, are manufactured. And further the CTBN modified epoxy composite laminates reinforced with intralayer hybrid carbon/aramid fabrics are successfully prepared. The influence of intralayer hybridization of carbon/aramid fibers with different braiding styles on in-plane impact properties of composite laminates is systematic analyzed by drop weight test, and then failure mode is also investigated by impact fracture morphology to further explain the impact resistance capacity.

Experimental

Materials and Preparation

The T700 carbon fiber yarns of 12 K and aramid fiber yarns of 1000 denier were selected to produce 2D&3D hybrid fabrics using easier single-wefted and double-wefted methods. Parameters of braiding fabric specimens were listed in Table 1. Figure 1(a)-(e) showed the surface morphology of 2D&3D braiding fabrics which had different architectures, where the specimen thickness was controlled from adjusting volume fraction of aramid fiber and braiding method in thickness direction. In addition, Figure 1(f)-(j) showed the constructed images of braiding fabrics with different styles by 3D models for showing the internal braiding structure of carbon-aramid intralayer hybrid fabrics. Diglycidyl ether of bisphenol A (DGEBA) (E-51) of epoxy equivalent 0.48-0.54 modified by liquid Carboxyle terminated polybutadiene (L-CTBN) was used as the matrix in this work. The photo initiator of 2-4 % triarylsulfonium hexafluoroantimonates (109037-75-4, under the commercial name of SIGMA-ALORICH) and thermal initiator of 10-15 % triethylene tetramine were used to cure the modified epoxy resins. Then the carbon-aramid hybrid/modified-epoxy braiding composites were prepared in the mold of 3000Pa pressure from the upper mould with stacking pattern alternately by hand lay-up technology, which the ply stacking number was two and three, according to the previous experimental results in our research group. Then the whole system was transferred into ultraviolet gej erator after vacuum deformation of 30 min. There were three cycles of ultraviolet irradiation with time of 60-80 s each cycle and 45 s each interval for triggering the double curing agents with about 1000 °C temperature, according to the related literature and a lot of experimental results [40-43], leading to the optimal performance of intralayer hybrid laminates. The composite laminates were obtained after 30 min curing at room temperature. The whole technological process of braided composites was revealed in Figure 2. The properties of obtained braiding laminates were summarized

Table 1. Parameters of 2D braided fabric specimens

	Thickness (mm)	Volume fraction of aramid fiber yarns (%)	Knitting style	Weaving method
a	0.74	0	Plain weave	Singe-wefted
b	0.78	25	Plain weave	Singe-wefted
c	0.85	33	Plain weave	Singe-wefted
d	1.05	50	Cross grain	Double-wefted
e	1.1	63	Cross grain	Double-wefted

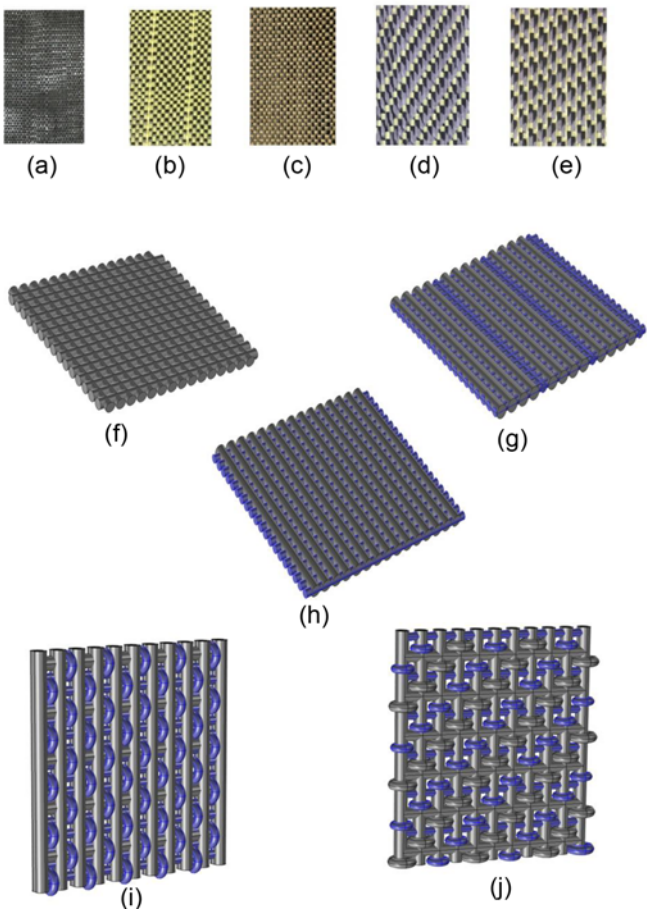

Figure 1. Surface picture and 3D models of braided fabrics: with different content of aramid fiber; (a, f) 0 %, (b, g) 63 %, (c, h) 50 %, (d, i) 33 %, and (e, j) 25 %.

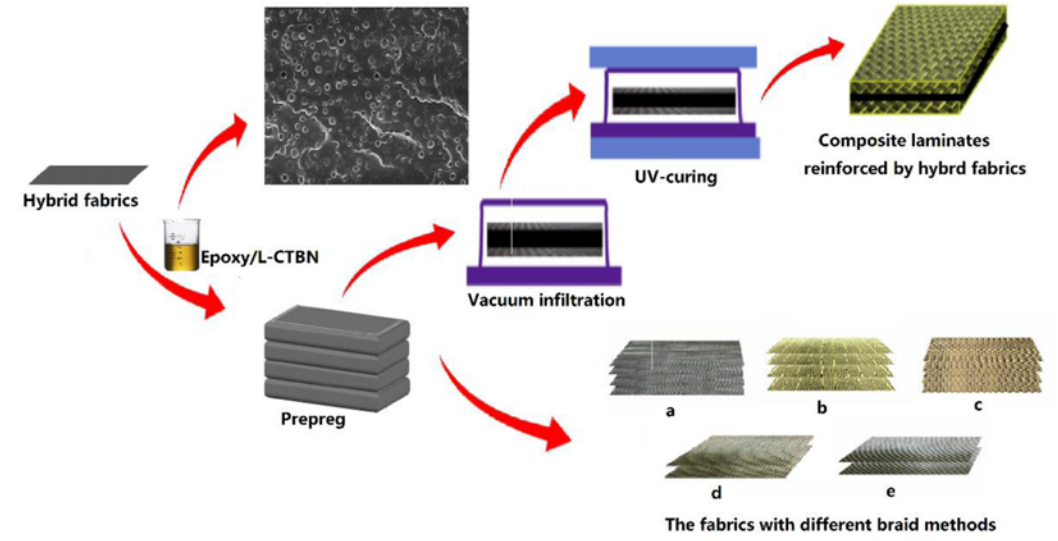

Figure 2. Whole technological process of braided composites.

Table 2. Character summary of epoxy composite laminates reinforced by different hybrid fibers

	Thickness (mm)	Ply stacking number	Density (g/cm^3)	Volume fraction of aramid fiber (%)
a	3.57	Three	1.36	0
b	3.68	Three	1.33	25
c	3.88	Three	1.28	33
d	3.86	Two	1.39	50
e	3.92	Two	1.22	63

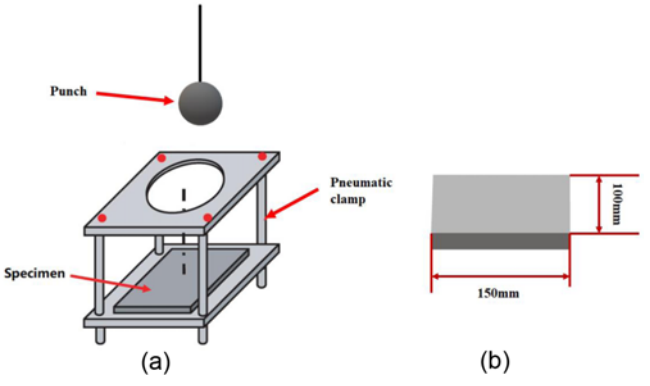

Figure 3. (a) 3D model of dropping hammer test machine and (b) size of specimen.

in Table 2.

Characterization and Testing

The braiding composite laminates were processed to the standard size of 110 mm×150 mm according to ASTM D7136/D7136M-2015 for impact test. Impact performance was carried out on MTS universal testing machine at an incidental impact energy of 26 J, the diameter and mass of impactor were 12.5 mm and 6.5 kg, respectively. The 3D model of dropping hammer test machine and size of specimen was showed in Figure 3. A minimum of 3 specimens were detected for each sample. The impact energy and falling height were calculated basing on the following formula (1) and (2):

$$E = C_E h \tag{1}$$

$$H = \frac{E}{m_d g} \tag{2}$$

where the E is the potential energy of punch, J; C_E is the ratio of standard impact energy to specimen thickness, J/mm; h represents the thickness of specimen, mm. H is the falling height; m_d and g represent the quality, kg, and gravity acceleration, respectively.

The braiding fabrics and damage fracture surface of impact test specimens were observed by using a Philips scanning electron microscope (SEM) at an accelerating voltage of 20 kV, specimens were coated with gold prior to imaging.

Results and Discussion

Different Braiding Structure of Fabrics by Single-wefted and Double-wefted Method

The fiber structure of 2D&3D fabrics with different braiding styles by easier single-wefted and double-wefted method is revealed in Figure 4. It's noteworthy that the advantage of 3D fabrics, which exists aramid fibers as the Z-

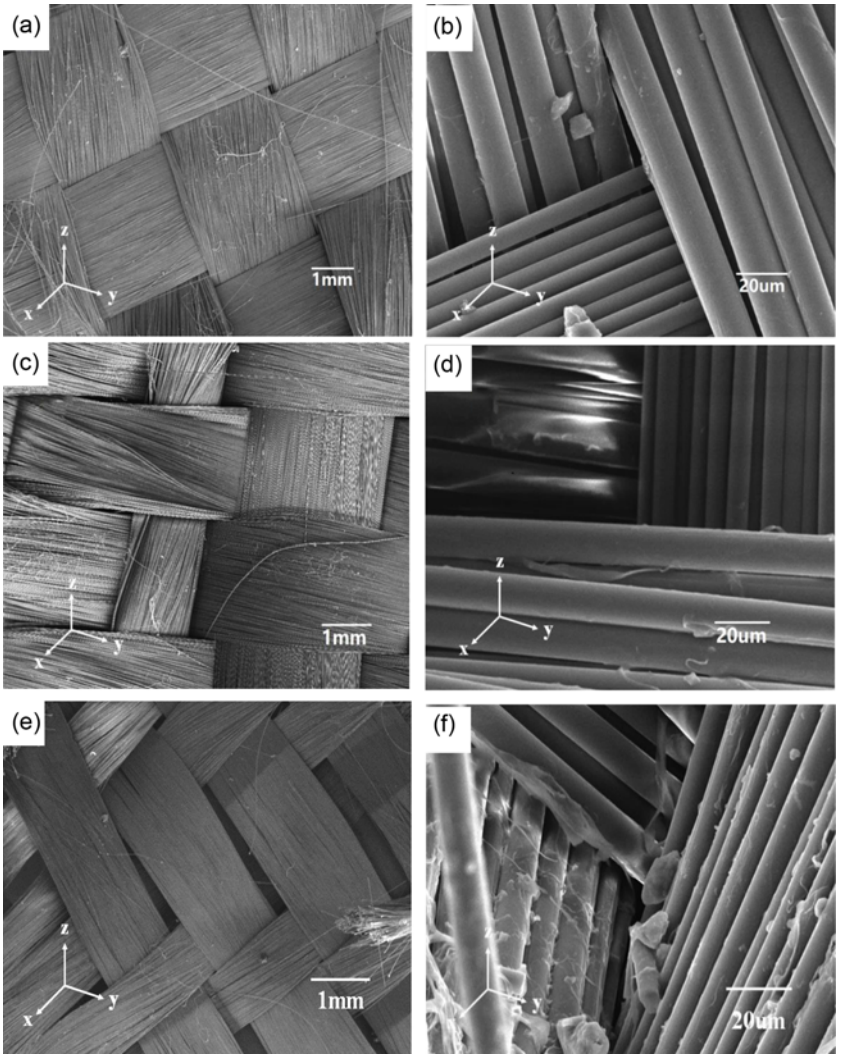

Figure 4. Fiber morphology with different weaving method of (a, b) 50 % aramid fibers by single-wefted, (c, d) 63 % aramid fibers by single-wefted, and (e, f) 25 % armid fibers by double wefted.

yarns along thickness direction manufactured by easier process and less cost, is observed. From Figure 4(a)-(d), the braiding fabrics by single-wefted method show 2D form that the warp and weft yarns in the direction of x and y are braided with orthometric straight alignment structure. However, the 3D braiding structure with double-wefted method is showed in Figure 4(e) and (f). As seen, the Z-yarns, that is made up of aramid fiber with higher toughness relative to the carbon fiber, can be obviously observed, compared to the fabrics with 2D structure by single-wefted method. The structure advantage of 3D fabrics indicates better impact resistance ability of braiding composite laminates, which is attributed to the Z-yarns have a significant influence on preventing the damage propagation due to a higher initial flexivity by introduction the aramid fibers in thickness direction. From Figure 4(a) and (b), the 2D fabrics containing 50 % aramid fibers present relatively compact structure, which also have a significance influence on the improvement of anti-impact performance, although there is not aramid fiber as the Z-yarns. It is mainly ascribed to perpendicular braiding structure and same proportion of carbon and aramid fibers, contributing to better synergistic effect of in-plane stiffness and flexivity of composite laminate, which delays the damage initiation and further propagation. However, it is still short of energy dissipation path of the Z-yarns, thus, the capacity of energy absorption and force transfer is still weaker than that laminates prepared with 3D fabrics. From the Figure 4(c) and (d), the 2D fabrics containing 63 % aramid fibers present loose structure with great interspace between aramid fiber and carbon fiber due to the difference of both fiber diameter and braiding style, which may suggest relatively weak impact resistance performance. Basing on the impact test instrument, the contact duration is long enough for the entire fabric architecture

to respond to the impact load, in consequence, more impact energy may be absorbed. Thus, the presence of Z-yarns of aramid fibers can prevent the damage propagation, leading to an improvement of inherent energy absorption and time of the impact force transmission, which indicates the optimal impact resistance of braiding laminates reinforced by fabrics with 3D structure by double-wefted method [44,45].

Impact Behavior of Carbon-aramid/epoxy Intralayer Hybrid Composite Laminates

Impact Peak Force of Composite Laminates Reinforced by Fabrics with Different Braiding Styles

To investigate the influence of different intralayer hybridization styles on in-plane impact properties, the drop-hammer impact test is conducted on braiding composites laminates. The typical force versus displacement responses for all five kinds of specimens at an incidental impact energy of 26 J are showed in Figure 5(a) to (e), respectively. A comprehensive depiction of damage initiation, propagation and the change of the specimen stiffness can be obtained from Figure 5. As seen, the first part of curve is linear and represents the stiffness of nondamaged specimen. Then, more force oscillations are observed before reaching the maximum of force due to the initiation and propagation of damage, leading to the stiffness reduction of braiding composite laminates. The force decreases after reaching the

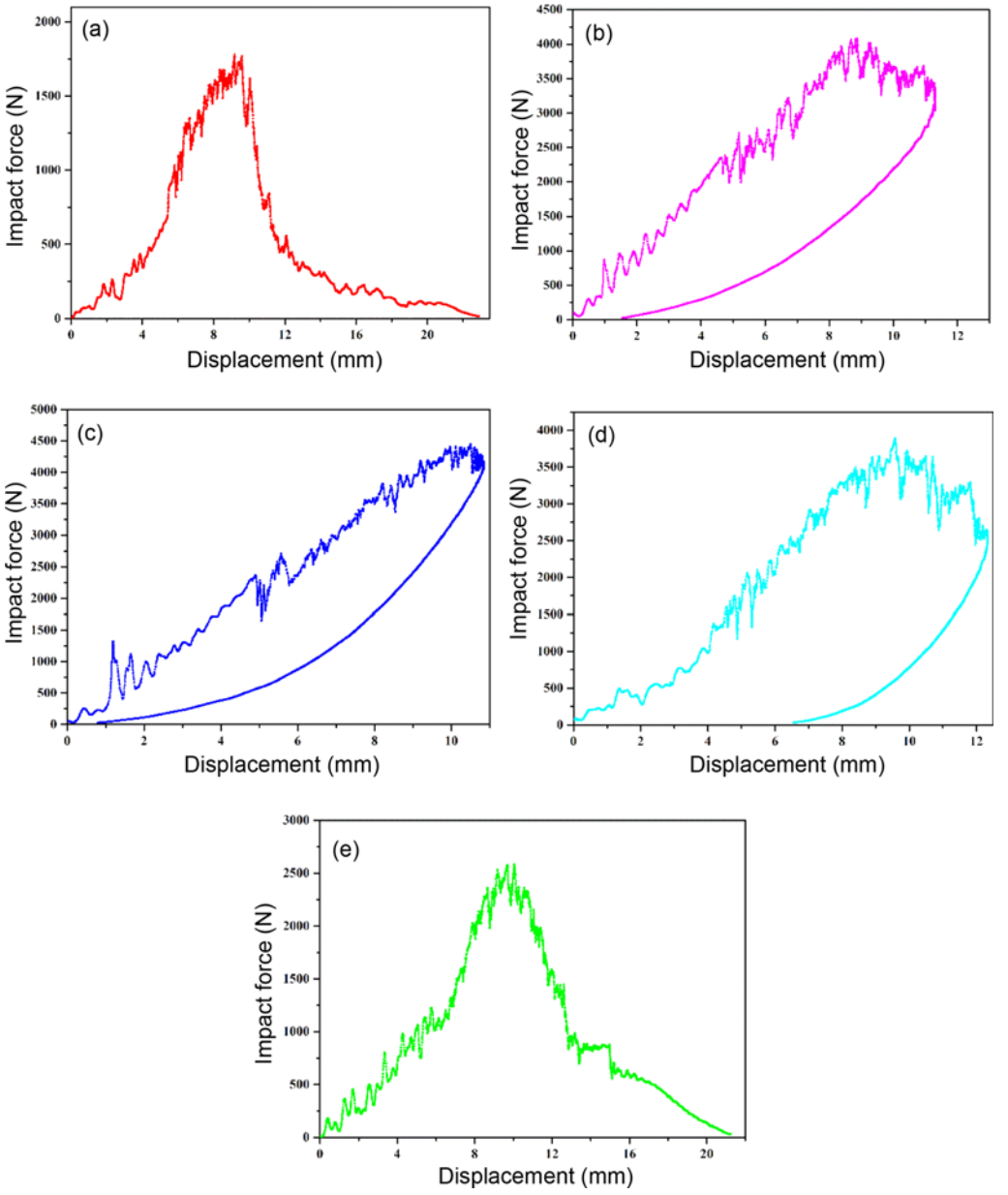

Figure 5. Impact force results of braid composite laminates; (a) 0 %, (b) 25 %, (c) 33 %, (d) 50 %, and (e) 63 %.

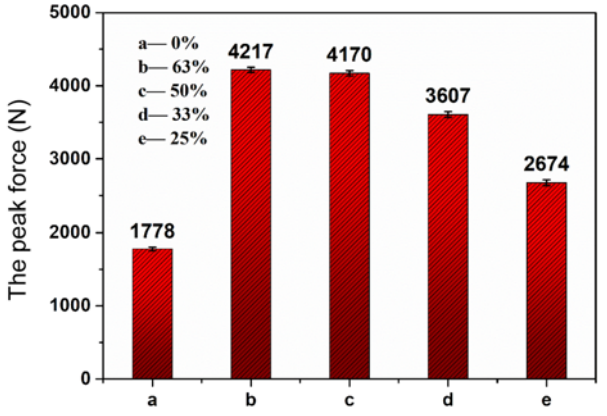

Figure 6. Impact peak force of braid composite laminates with different addition of aramid fibers.

highest value, which can be attributed to the critical structure damage. Then there is a force redistribution of the surviving composite laminates until the impact load is removed [46-48].

The peak force under the same impactor is an indicator of the load buffering capacity of the braiding laminates, directly related to the initial rigidity of specimens. Figure 6 shows the results of impact peak force. As seen, it is obviously that the peak force of braiding composite reinforced by pure carbon fabrics is 1778 N, while higher values are obtained by the carbon-aramid intralayer hybrid composite laminates. The braiding laminate with the 3D fabric style of containing 25 % aramid fibers by double-wefted method presents the optimal anti-impact performance, and the peak force reaches 4217 N, increased by 137.2 %

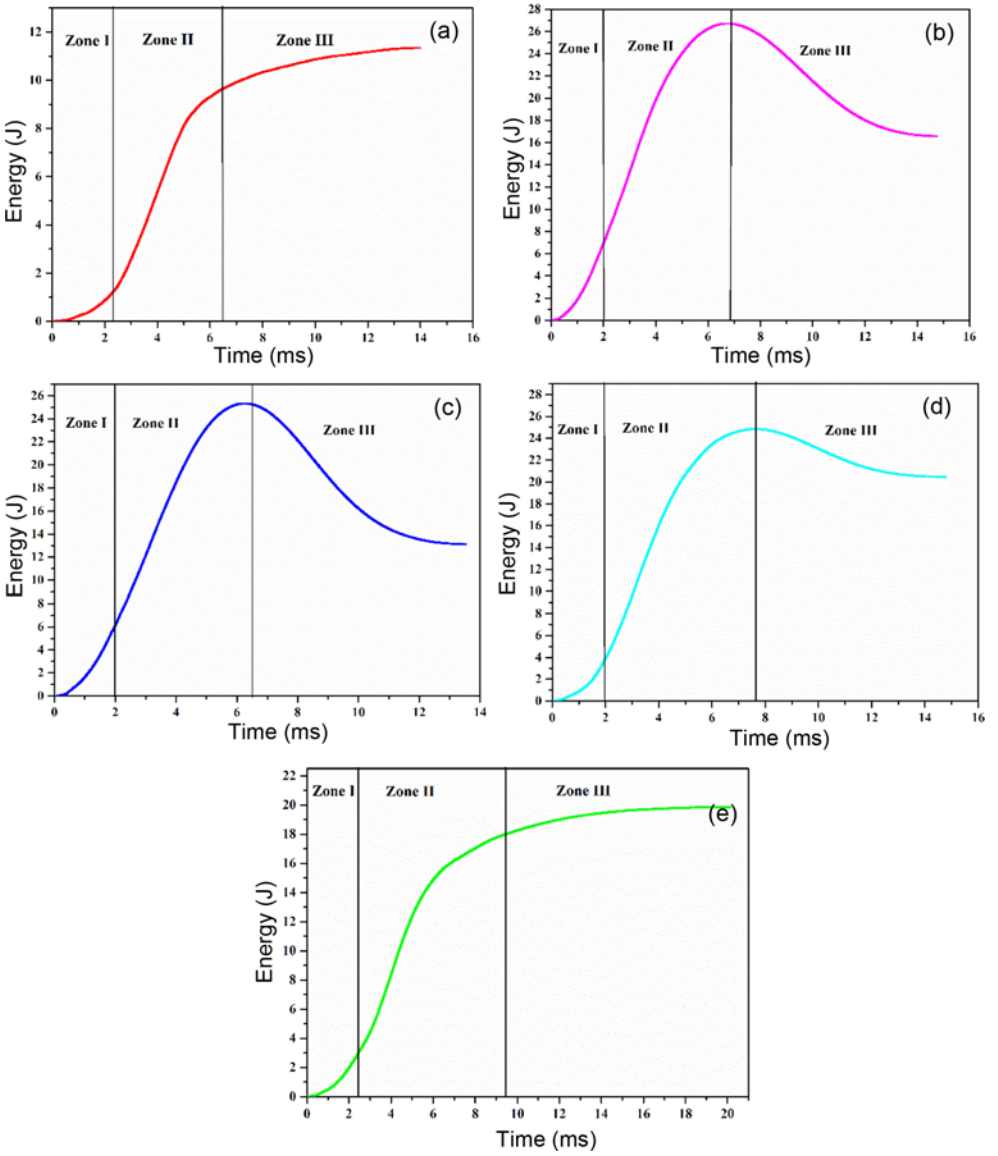

Figure 7. Impact absorbed energy of braid composite laminates; (a) 0 %, (b) 25 %, (c) 33 %, (d) 50 %, and (e) 63 %.

relative to pure carbon laminate. And the specimens c manufactured by 3D fabric containing 33 % aramid fiber also shows better anti-impact performance, the peak force is 4170 N. And then, the peak force of d, e, with 2D fabric style by incorporation of 50 %, 63 % aramid fibers, arrives at 3607 N, 2674 N, respectively, which also are better than the pure carbon laminate. It is attributed to the addition of higher strain-to-failure aramid fibers by 2D&3D fabric styles that helps in improving plastic deformation, which can lead to an increase in the load sharing capacity of the structure. Thus, the cushioning effect offered by aramid fibers has a positive influence on the improvement of impact resistance. And, the results also show that 3D fabrics have superior effect on enhancement of anti-impact performance relative to the 2D fabrics due to the introduction the aramid fiber as Z-yarns, which is agreed with the analysis of fabric structure. In addition, the anti-impact properties of braiding composites start to decrease with the addition of more than 25 % aramid fibers. That shows carbon fiber with higher modulus also play an important role for damage initiation, because it decides the initial stiffness of braiding laminates. Thus, there exists an optimal proportion of aramid fiber for increasing the impact resistance performance. And the initial in-plane stiffness determines the impact resistance capacity of the braiding composite laminates. So, the intralayer hybrid laminate with the style of containing 25 % aramid fibers by double-wefted braiding method, that reach the highest penetration forces as well as sustain this peak force for a much longer duration due to the optimal style design, shows optimal anti-impact performance.

Impact Absorbed Energy of Composite Laminates Reinforced by Fabrics with Different Braiding Styles

Figure 7 exhibits the curve trend of absorbed energy versus time of braiding composite laminates. It can be seen that the curves show similar trend and present the shape of inverse S, and it can be characterized with three distinct zones [49-51]. At the first stage (Zone I), the absorbed energy slowly increases and values are relatively low. It may be attributed to the small dent and deformation damage along the thickness direction under the in-plane impact load. For second stage (Zone II), the curves of energy versus time exhibit an increase in slope, demonstrating an augment in flexivity of braiding composites with internal fracture damage. It can be suggested that the curve trend is mainly due to the increase of contact area between the impactor and the braid laminates. As last stage (Zone III), the absorbed energy maintains a constant value, which is attributed to the completely damage in the thickness direction of braid composite laminates.

The maximum values of impact absorbed energy are summarized in Figure 8. As seen, the absorbed energy of hybrid laminate reinforced by pure carbon fibers is only 11.34 J, however, for the specimen b, c, d and e, it reaches 26.71 J, 25.32 J, 24.83 J, and19.86 J, increased by 135.5 %, 123.2 %, 119.0 % and 75.1 %, respectively. The 3D fabric style with 25 % aramid fiber reveals optimum load sharing capacity, which is agreed with the peak force results. Thus, it indicates that the carbon and aramid fibers preferably play synergistic effect on resisting the shock due to their optimal braiding style again. That is to say the performance of braiding composites in terms of stiffness and flexivity of braiding composite maintains a nice balance for energy absorption due to the introduction of 3D style by easier double-wefted method, which contribute to better impact resistance ability.

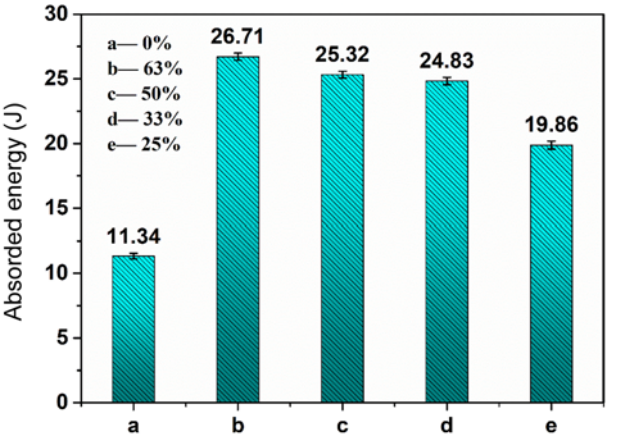

Figure 8. Absorbed energy of braid composite laminates with different addition of aramid fibers.

Impact Damage Mechanism of Composite Laminates Reinforced by Fabrics with Different Braiding Styles

The impact fracture morphology of braiding composite laminates is showed in Figure 9. From Figure 9(a), a great deal of fractured carbon fibers can be easily found, and there are a few debonding and bending of carbon fiber. Thereby, the fiber fracture is the main damage mode for pure carbon fabric braid laminates, showing the poor behavior in anti-impact properties due to the weaker in-plane properties of carbon fibers. While the laminates reinforced by 3D fabrics present similar fracture morphology. From Figure 9(b) and (c), a great deal of kinking, necking and deflection of aramid fibers can be found, indicating introduction of aramid fiber in thickness direction makes it work better in anti-impact performance due to increasing the energy dissipation path of braiding laminates. It does not almost find about the fracture of carbon fiber, which is attributed to the aramid fibers as Z-yarns increasing the energy absorption and force transfer by fiber-bridging and necking, preventing the damage of carbon fibers. The damage modes in terms of fiber fracture, kinking and necking of carbon and aramid fibers are clearly observed in braiding laminates reinforced by 2D fabrics with the 1:1 ratio of carbon and aramid fibers. Moreover, the matrix debonding also is presented in the Figure 9(d).

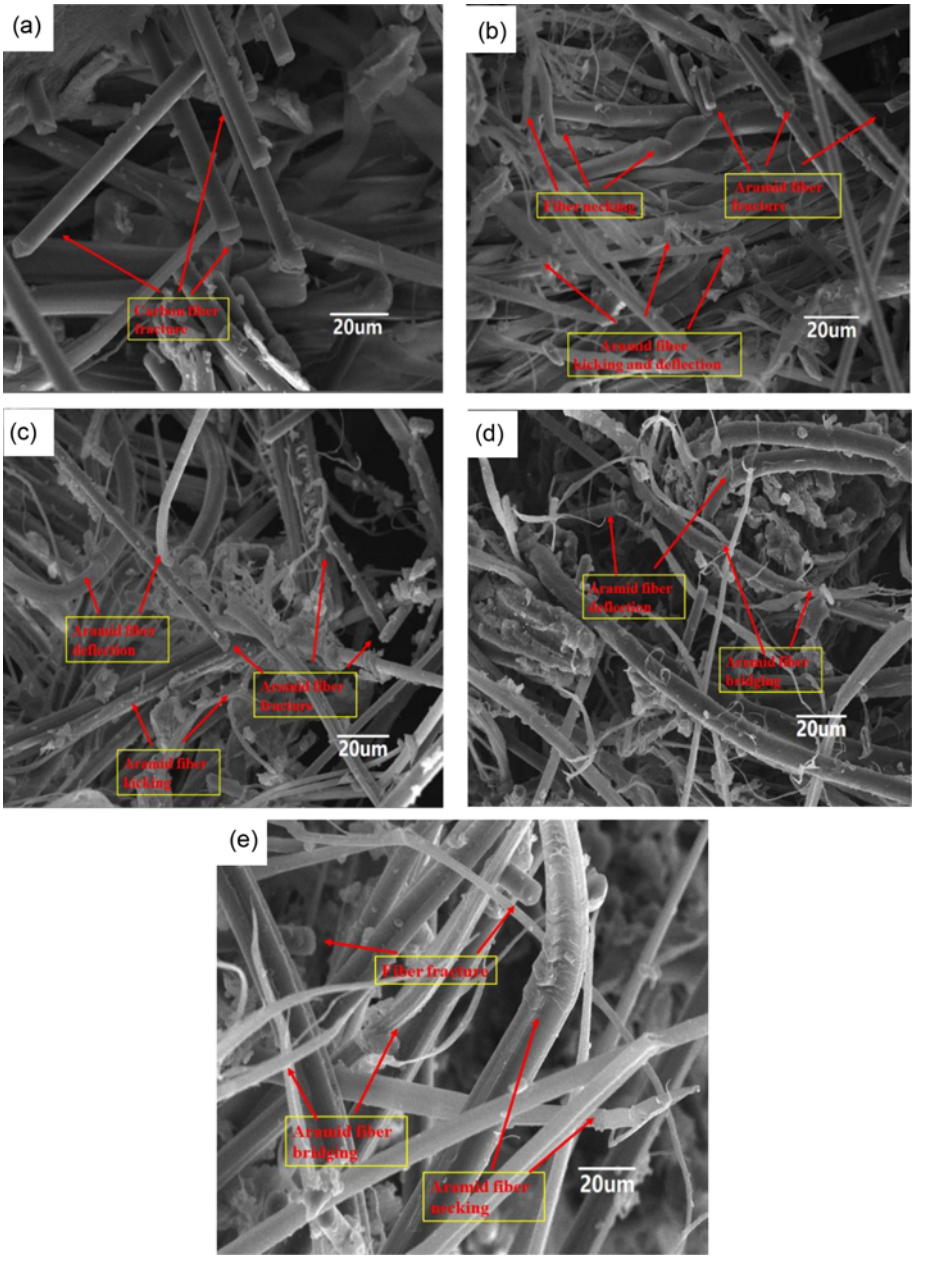

Figure 9. Impact fracture morphology of braid composite laminates; (a) 0 %, (b) 25 %, (c) 33 %, (d) 50 %, and (e) 63 %.

Thereby, carbon and aramid fibers as well as the modified epoxy matrix have an important effect on improvement of resistance impact capacity, simultaneously, and then, the relatively good anti-impact performance can be obtained. For the specimen (e), the main damage modes are the fiber-bridging and necking of aramid fibers, however, few fiber fracture of carbon fiber also is observed. The analysis is in agreement with the above results of impact performance, indicating the aramid fibers have a significant effect on the improvement of impact resistance, in particular, the introduction of aramid fiber in thickness direction by 3D style. It is mainly ascribed to two stresses spread along both the in-plane fiber and the through-thickness direction. The energy dissipation mechanism in the thickness direction is enhanced due to the aramid fibers as Z-yarns, and it effectively prevents the more damage propagation from occurring, contributing to optimal impact resistance capacity. In addition, there exists the suitable percentage of aramid fibers and carbon fibers, which plays a synergistic effect for improving the impact resistance ability.

Whereas the investigation of laminates still is insufficient from the impact results and fracture morphology. Next, the

forthcoming research will focus on the manufacturing of thicker 3D fabrics making the laminates prepared by only one 3D fabric, further reducing the number of interfaces, which ensures the better performance of composite laminates. And the 3D hybrid laminates are the optimal repairing patches for the damaged aluminum alloy from the aircraft and automobile, which can decrease much cost due to the abandon of equipment. Thus, the laminates reinforced by 3D fabrics with better performance will have a significant influence on the related industry areas.

Conclusion

The CTBN-EP composite laminates reinforced by braiding fabrics with different 2D&3D styles were successfully prepared. The effect of fabrics with different braiding styles on impact performance of its reinforced epoxy composite laminate was investigated by drop-weight impact test. The detailed results were summarized in next.

1. The anti-impact performance of intralayer hybrid composite laminates were obviously enhanced due to the incorporation of aramid fibers.
2. The composite laminates reinforced by 3D style fabrics showed the optimal impact performance, and the impact peak force and energy reach 4217 N and 26.71 J, increased by 137.18 % and 135.54 % relative to pure carbon laminates.
3. From the braiding structure of fabrics and fracture morphology, the aramid and carbon played a synergistic effect for improving the impact resistance ability.
4. It existed more energy dissipation paths for 3D fabrics due to the introduction of aramid fiber as the Z-yarns, contributing to the optimal anti-impact performance of composite laminates.

Acknowledgements

This work was financially supported by the National Defense Foundation of China.

References

1. M. Holmes, *Reinf. Plast*., **57**, 24 (2013).
2. B. Liu, Z. Liu, X. Wang, S. Long, and J. Yang, *Polym. Test*., **32**, 724 (2013).
3. N. Nistico, J. Ozbolt, and G. Polimanti, *Compos. Part B*., **90**, 351 (2016).
4. D. W. Y. Wong, L. Lin, P. T. McGrail, T. Peijs, and P. J. Hogg, *Compos. Part A.,* **41**, 759 (2010).
5. S. T. Pinho, P. Robinson, and L. Iannucci, *Compos. Sci. Technol*., **66**, 2069 (2006).
6. J. Lee and C. Soutis, *Compos. Sci. Technol.,* **68**, 2359 (2008).
7. A. Yudhanto, N. Watanabe, Y. Iwahori, and H. Hoshi, *Compos. Sci. Technol*., **86**, 52 (2013).
8. M. Bocciarelli, S. Gambarelli, N. Nistico, M. A. Pisani, and C. Poggi, *Compos. Part B*., **67**, 9 (2014).
9. R. D. Crouch, S. B. Clay, and C. Oskay, *Compos. Part B*., **48**, 59 (2013).
10. A. Yudhanto, N. Watanabe, Y. Iwahori, and H. Hoshi, *Compos. Sci. Technol*., **86**, 52 (2013).
11. H. Saghafi, S. R. Ghaffarian, D. Salimi-Majd, and H. A. Saghafi, *Compos. Struct*., **166**, 49 (2017).
12. V. H. Mahesh, C. A. Farhan, and J. Shaik, *J. Compos. Mater*., **41**, 2195 (2007).
13. H. Saghafi, T. Brugo, G. Minak, and A. Zucchelli, *Procedia Eng*., **88**, 109 (2014).
14. H. Saghafi, R. Palazzetti, A. Zucchelli, and G. Minak, *Eng. Solid. Mech*., **1**, 85 (2013).
15. P. Akangah, S. Lingaiah, and K. Shivakumar, *Compos. Struc*., **92**, 1432 (2010).
16. S. Kravchenko, O. Kravchenko, M. Wortmann, M. Pietrek, P. Horst, and R. B. Pipes, *Compos. Part A*., **54**, 98 (2013).
17. N. Naik, R. Ramsimha, H. Arya, S. Prabhu, and N. Shamarao, *Compos. Part B*., **32**, 565 (2001).
18. A. Enfedaque, J. M. Molina-Aldareguía, F. Gálvez, C. González, and J. Lorca, *J. Compos. Mater*., **44**, 3051 (2010).
19. A. Balaji, B. Karthikeyan, J. Swaminathan, and C. Sundar Raj, *Fiber. Polym*., **18**, 1193 (2017).
20. A. Balaji, B. Karthikeyan, J. Swaminathan, and C. Sundar Raj, *Int. J. Polym. Anal. Ch*., **18**, 70 (2018).
21. H. S. Ju, *Compos. Part B*., **79**, 61 (2015).
22. G. Pincheira, C. Canales, and C. Medina, *P. I. Mech. Eng. L-J Mat*., **10**, 1177 (2015).
23. H. Sezgin and O. B. Berkalp, *J. Ind. Text*., **47**, 283 (2016).
24. S. A. Tekalur, K. Shivakumar, and A. Shukla, *Compos. Part B*., **39**, 57 (2008).
25. M. Kuwata and P. J. Hogg, *Compos. Part A*., **42**, 1551 (2011).
26. C. Ayranci and J. Carey, *Compos. Struct.*, **85**, 43 (2008).
27. X. G. Yu and J. Z. Cui, *Compos. Sci. Technol*., **67**, 471 (2007).
28. V. Fiore, T. Scalici, F. Sarasini, J. Tirillo, and L. Calabrese, *Compos. Part B*., **116**, 99 (2017).
29. K. B. Aswani, K. M. Vijay, A. Suhail, and B. Naresh. *Polym. Test.*, **61**, 396 (2017).
30. J. N. Baucom and M. A. Zikry, *J. Compos. Mater*., **37**, 1651 (2003).
31. B. Vieille, V. M. Casado, and C. Bouvet, *Compos. Struct*., **101**, 9 (2013).
32. R. Seltzer, C. González, R. Muñoz, J. LLorca, and T. Blanco-Varela, *Compos. Part A*., **45**, 49 (2013).
33. K. J. Kim, W. R. Yu, J. S. Lee, L. Gao, E. T. Thostenson, T. W. Chou, and J. H. Byun, *Compos. Part A*., **41**, 1531 (2010).
34. PJ. Liotier, V. Alain, and D. Christine, *Compos. Part A*., **41**, 653 (2010).

35. G. A. Schoeppner and S. Abrate, *Compos. Part A*., **31**, 903 (2000).
36. Y. Y. Li, B. Z. Sun, and B. H. Gu, *Compos. Struct*., **176**, 43 (2017).
37. O. Dorival, P. Navarro, S. Marguet, C. Petiot, M. Bermudez, D. Mesnagé, and J. F. Ferrero, *Compos. Part B*., **78**, 244 (2015).
38. H. Ullah, A. R. Harland, and V. V. Silberschmidt, *Compos. Sci. Technol*., **92**, 55 (2014).
39. H. Huang and M. W. Anthony, *Compos. Sci. Technol*., **69**, 2338 (2009).
40. M. Sangermano, M. Periolatto, V. Signore, and P. R. Spena, *Prog. Org. Coat*., **103**, 152 (2017).
41. J. P. Zhou, S. J. Jia, W. L. Fu, Z. L. Liu, and Z. Y. Tan, *Mater. Lett*., **176**, 228 (2016).
42. J. H. Lu and J. P. Youngblood, *Compos. Part B*., **82**, 221 (2015).
43. J. J. Xi, X. Y. Liu, Z. Q. Yu, and J. Sandw, *Struct. Mater*., **22**, 1 (2018).
44. Y. Shi, T. Swait, and C. Soutis, *Compos. Struct*., **94**, 2902 (2012).
45. N. H. Nash, T. M. Young, P. T. McGrail, and W. F. Stanley, *Mater. Des.*, **85**, 582 (2015).
46. C. Evci and M. Gulgec, *Int. J. Impact. Eng.*, **43**, 40 (2012).
47. M. V. Hosur, M. Adbullah, and S. Jeelani, *Compos. Struct*., **67**, 253 (2005).
48. D. T. Zhang, Y. Sun, L. Chen, and N. Pan, *Mater. Des*., **50**, 750 (2013).
49. E. Sevkat, B. Liaw, F. Delale, and B. B. Raju, *Compos. Part B*., **41**, 403 (2010).
50. C. Thanomsilp and P. J. Hogg, *Compos. Sci. Technol*., **63**, 467 (2003).
51. S. Erdem, P. Prasad, H. Paul, and S. Costas, *Compos. Part B*., **91**, 522 (2016).